Downloaded from orbit.dtu.dk on: Jan 23, 2019

DTU Library

Optical properties and surface characterization of pulsed laser-deposited Cu2ZnSnS4 by spectroscopic ellipsometry

Crovetto, Andrea; Cazzaniga, Andrea Carlo; Ettlinger, Rebecca Bolt; Schou, Jørgen; Hansen, Ole

Published in:
Thin Solid Films

Link to article, DOI:
10.1016/j.tsf.2014.11.075

Publication date:
2015

Document Version
Peer reviewed version

Link back to DTU Orbit

Citation (APA):
Crovetto, A., Cazzaniga, A. C., Ettlinger, R. B., Schou, J., & Hansen, O. (2015). Optical properties and surface characterization of pulsed laser-deposited Cu2ZnSnS4 by spectroscopic ellipsometry. Thin Solid Films, 582, 203-207. DOI: 10.1016/j.tsf.2014.11.075

General rights
Copyright and moral rights for the publications made accessible in the public portal are retained by the authors and/or other copyright owners and it is a condition of accessing publications that users recognise and abide by the legal requirements associated with these rights.

- Users may download and print one copy of any publication from the public portal for the purpose of private study or research.
- You may not further distribute the material or use it for any profit-making activity or commercial gain
- You may freely distribute the URL identifying the publication in the public portal

If you believe that this document breaches copyright please contact us providing details, and we will remove access to the work immediately and investigate your claim.

Manuscript for proceedings of Symposium A "Thin film chalcogenide photovoltaic materials" at E-MRS 2014 Spring Meeting

Key: 9OQVO

Optical properties and surface characterization of pulsed laser-deposited Cu_2ZnSnS_4 by spectroscopic ellipsometry

Andrea Crovetto[(1)*], Andrea Cazzaniga[(2)], Rebecca B. Ettlinger[(2)], Jørgen Schou[(2)] and Ole Hansen[(1,3)]

[(1)] DTU Nanotech, Technical University of Denmark, DK-2800 Kgs. Lyngby, Denmark

[(2)] DTU Fotonik, Technical University of Denmark, DK-4000 Roskilde, Denmark

[(3)] CINF, Center for Individual Nanoparticle Functionality, Technical University of Denmark, DK-2800 Kgs. Lyngby, Denmark

[*]: corresponding author. Address: DTU Nanotech, Ørsteds Plads, building 344, room 030, DK-2800 Kgs. Lyngby, Denmark phone: +45 45255845, fax: +45 45887762, email: ancro@nanotech.dtu.dk

Optical properties and surface characterization of pulsed laser-deposited Cu_2ZnSnS_4 by spectroscopic ellipsometry

Andrea Crovetto[(1)], Andrea Cazzaniga[(2)], Rebecca B. Ettlinger[(2)], Jørgen Schou[(2)] and Ole Hansen[(1,3)]

[(1)] DTU Nanotech, Technical University of Denmark, DK-2800 Kgs. Lyngby, Denmark

[(2)] DTU Fotonik, Technical University of Denmark, DK-4000 Roskilde, Denmark

[(3)] CINF, Center for Individual Nanoparticle Functionality, Technical University of Denmark, DK-2800 Kgs. Lyngby, Denmark

Abstract

Cu_2ZnSnS_4 films prepared by pulsed laser deposition at different temperatures are characterized by spectroscopic ellipsometry. The focus is on confirming results from direct measurement techniques, by finding appropriate models of the surface overlayer for data fitting, and extracting the dielectric function of the films. It is found that the surface overlayer changes with film thickness and deposition temperature. Adopting different ellipsometry measurement and modeling strategies for each film, dielectric functions are extracted and compared. As the deposition temperature is increased, the dielectric functions exhibit additional critical points related to optical transitions in the material other than absorption across the fundamental band gap. In the case of a thin film < 200 nm thick, surface features observed by scanning electron microscopy and atomic force microscopy are accurately reproduced by ellipsometry data fitting.

1. Introduction

Cu_2ZnSnS_4 (CZTS) is a promising candidate to replace commonly used thin-film solar cell absorbers $Cu(In,Ga)Se_2$ (CIGS) and CdTe, which contain expensive or toxic materials. Unlike CIGS- and CdTe-

based solar cells, which have surpassed 20% power-conversion efficiencies on the laboratory scale, the current records for CZTS are 8.4% in the case of a sulfur-pure material [1] and 12.6% if S is alloyed with Se [2]. In order to improve the efficiency, both technological issues and a still incomplete understanding of the material need to be addressed. This includes for example the spectral optical properties of CZTS, which can help clarify its band structure and absorption behavior but have seldom been reported in the literature. Levcenko *et al.* [3] showed the dielectric function of bulk CZTS crystals using ellipsometry and a two-phase (substrate-layer) model. Li *et al.* [4] extracted the dielectric function of nanocrystalline films from transmittance spectra using a Tauc-Lorentz oscillator. Sun *et al.* [5] derived the absorption coefficient and band-gap energy of CZTS films from ellipsometry measurements. Finally, Li *et al.* [6] obtained the dielectric function of a CZTS film from ellipsometry data taken at multiple angles of incidence from both sides of the sample; the data was fitted with a dielectric function of arbitrary shape, without underlying physical assumptions. In this study we characterize CZTS films by spectroscopic ellipsometry, focusing on cross-checking results from direct measurement techniques and on determining the dielectric function in films exhibiting different levels of crystallization.

2. Experimental details

Films of CZTS were deposited on fused silica substrates by pulsed laser deposition (PLD) at different temperatures: two samples at 25°C (with different thicknesses, named C-25t and C-25T), one at 350°C (C-350) and one at 425°C (C-425). A sintered Cu_2ZnSnS_4 target was used (PVD Products). The laser wavelength, fluence and pulse repetition rate were 248 nm, 3 J/cm^2 and 15 Hz respectively. The background pressure was 7×10^{-7} mbar and the target-to-substrate distance was 40 mm. The film surface was imaged with a scanning electron microscope (SEM) equipped with a field emission gun and an in-

lens secondary electron detector (FE-SEM, Supra 40VP, Zeiss) by tilting the sample to 45°. Energy dispersive X-ray spectroscopy (EDX) was performed in the same instrument using a silicon drift detector (X-Man^N 50, Oxford Instruments) and a beam voltage of 15 kV. Surface roughness was measured by stylus profiling (Dektak 8, Veeco) and atomic force microscopy (AFM, Dimension 3100, Bruker AXS) using tapping mode. The root-mean-square surface roughness (R_q) is employed in this work. X-ray diffraction (XRD) patterns were collected with a BrukerD8 powder diffractometer in Bragg-Brentano configuration using Cu-Kα radiation. Raman spectra were obtained at a laser wavelength of 455 nm, laser power of 0.4 mW and spot size of 1 μm^2 in the backscattering configuration (DXR Raman Microscope, Thermo Scientific). Ellipsometric measurements were performed in the spectral range 0.7-5.9 eV on a rotating compensator spectroscopic ellipsometer (M-2000, J.A. Woollam Co.) using seven angles of incidence (from 45 to 75°) and a collimated beam.

3. Results and discussion

3.1. Preliminary analysis

Energy dispersive X-ray spectroscopy (EDX) demonstrated that all films are Cu- and Sn-rich.
The films deposited at 25°C showed no XRD peaks (Fig. 1) and no crystal grain contrast in the scanning electron microscope (SEM) images (Fig. 2(a,b)). However, the peaks associated with CZTS were present in their Raman spectra (Fig. 3). Since Raman spectroscopy is more sensitive to the crystal short-range order than XRD [7] it can be assumed that these films have very small grains and/or are only partially crystallized. At 350°C a nanocrystalline grain structure becomes visible in the SEM and is detected by XRD, with an average grain diameter of 50 nm (partially visible in Fig. 2(c)). At 425°C the film is crystalline with an average grain diameter of about 200 nm (estimate based on morphology, Fig. 2(d)).

3.2. Analysis of surface overlayer

The surface overlayer is often difficult to model when fitting ellipsometry data [8] so it is helpful to gain some knowledge from other techniques. As shown in the SEM images in Fig. 2, the film surface is heterogeneous for all our samples. Except for C-425, the films have some localized protrusions, typically in the form of nanospheres (inset graph in Fig. 2(a)) on top of a relatively smooth surface. Surface roughnesses, measured by a stylus profiler and AFM, are shown in Table 1. The overall surface roughness increases with film thickness but appears to be independent of the temperature, i.e. of the degree of crystallization and grain size. However, if the roughness is measured over an area without nanospheres (denoted film roughness in Table 1), the value increases with temperature until, at 425°C, it is impossible to make a distinction between the two definitions.

To verify if the surface region contains various phases besides being rough, Raman spectroscopy was employed. From ellipsometry measurements the absorption coefficient α of our CZTS films at the Raman laser wavelength of 455 nm is in the 1.5 - 2.0×10^5 cm^{-1} range. The Raman information depth is defined as the depth d such that $2d\alpha = 1$, i.e. half the optical penetration depth because the optical path of backscattered light in the material is doubled. Hence in our CZTS films 60% of the Raman signal originates within 25-35 nm below the surface, making the technique very surface sensitive at this wavelength. The laser spot size was directed onto one of the bigger nanostructures (the only ones clearly visible with an optical microscope) and the focus was adjusted first to the film surface, then to the top of the structure. The results are shown in the inset graph of Fig. 3 for the C-25t film, but similar results have been obtained for the other films in this study. When the laser is focused on the film surface the only visible peaks are the two main CZTS peaks (289 and 334 cm^{-1}) and a small peak at 316 cm^{-1} which could be Cu_3SnS_4 or SnS_2. When the focus is moved to the top of the structure, the relative

intensity of the two CZTS peaks is redistributed, the peak at 316 cm^{-1} disappears and a broad peak centered at 475 cm^{-1} appears, probably corresponding to a disordered $Cu_{2-x}S$ phase. This is supported by EDX spot analysis performed on the larger nanostructures, which consistently show an increase in the Cu fraction by 30-50% (relative) with respect to spot analysis on the smooth surface. To conclude, the surface overlayer consists both of a complex topography and of a different phase mix with respect to the underlying film.

3.3. Ellipsometry analysis

3.3.1. Optical modeling

Results from characterization techniques presented in the previous sections have been used as a starting point in building the optical layer stacks shown in Fig. 4 for ellipsometry data fitting. Based on the magnitude of the x-rays peaks from the substrate, the sampling depth of our EDX experiments is roughly estimated as around 500 nm, whereas the sampling depth of the XRD measurements is a few μm at all incidence angles. Therefore, EDX and XRD can help identify phases, and hence the dielectric function, of the bulk homogeneous film layer defined in the model. We expect to have a dominant CZTS component and smaller contributions from SnS and Cu_3SnS_4 (at least in C-350 and C-425). SEM imaging with secondary electrons and Raman spectroscopy both have sampling depths of a few tens nm in our experiments. Therefore, SEM images have been used to define the morphology of the surface overlayer in the optical model, i.e. a mix of air and a solid phase (Fig. 4). Raman spectroscopy, on the other hand, allows to confirm whether the dielectric functions of the surface overlayer and of the near-surface region are realistic. As previously mentioned, we expect a major contribution from $Cu_{2-x}S$. Raman experiments have also been performed on the cross sections of the two thicker films (C-25T and C-425) to complement XRD for bulk phase analysis. The intensity ratios of the peaks in cross-sectional

spectra are very similar to the ones in the corresponding surface spectra shown in Fig. 3, so it is assumed that the phase mix in the bulk of the film is not depth-dependent and hence the bulk film layer in the optical model should not be defined as a graded layer. All phases detected by XRD were detected by Raman spectroscopy, and the latter provided the additional information that Cu_3SnS_4 is also present in the C-25t sample and possibly in the C-350 sample (Fig. 3).

Based on the above discussion, the bulk film layer in the optical model should ideally be modeled as a mix of all phases expected in the bulk. As a first approximation, it could be a CZTS/SnS mix. However, a high correlation error was consistently found in the mixing ratio and dielectric function parameters, even when using literature dielectric functions of CZTS and SnS as initial parameters in the fitting algorithm. Therefore, it was decided to keep the film layer as a single-phase material in the model. It is then clear that the fitted dielectric functions are, to some degree, a mix of the dielectric functions of all phases present in the bulk. However, based on XRD and Raman measurements, we expect CZTS to be the main component.

3.3.2. Sample grown at 25°C (thin)

The C-25t sample is the simplest to analyze due to its lower surface roughness and its lack of long-range crystal order, which makes its dielectric function simpler to model. The optical model used to fit the data consists of: a mixed air-solid phase overlayer (the mix between the two being a fitting parameter), a homogeneous film, and a fused silica substrate (Fig. 4(a)). The fused silica substrate is fitted in all samples with a Sellmeier model [8]. The optical functions of the film and of the overlayer are both parameterized with a Tauc-Lorentz expression, typical of amorphous materials [9], but they are kept independent from each other. The overlayer is defined as partially depolarizing, with the depolarization fraction being a fitting parameter. It is found that, if only the three higher incidence angles (65°, 70°, and 75°) are used, the mean square error (MSE) is more than twice that obtained if

only the three lower angles are used (45°, 50°, and 55°), and it also results in generally higher correlated errors and larger deviation of the known parameters from their expected values. The same occurs if all available angles are used. Therefore, only the three lower angles are fitted (Fig. 5). The resulting topographic characteristics are shown in Table 1: they are in good agreement with the measurements from direct techniques also shown in Table 1. The surface overlayer is 53 nm thick (in good agreement with the inset in Fig. 2(a)) and consists of a mix of air (90 %) and a solid phase (10 %). This roughly corresponds to what is visible in the SEM image (Fig. 2(a)). The Tauc band gap of the CZTS film is 1.527 ± 0.003 eV, consistent with typical values reported in the literature [1,5]. The Tauc gap of the overlayer material is 2.07 ± 0.09 eV, which is consistent with a $Cu_{2-x}S$ phase since band gap energies between 1.7 eV and 2.7 eV have been reported for amorphous $Cu_{2-x}S$ [10,11].

3.3.3. Sample grown at 25°C (thick)

The C-25T sample is modeled with the same layer stack but this time the dielectric function of the CZTS film layer is a free parameter to vary without any pre-determined oscillator (Fig. 4(b)). The only physical assumptions are Kramers-Kronig consistency and an initial shape before fitting, chosen to be the Tauc-Lorentz function of sample C-25t. This gives a large number of fitting parameters, and it is found that correlation errors and consistency with thickness and roughness measurements are minimized using five incidence angles (45°-65°). The resulting dielectric function is similar to a Tauc-Lorentz function (comparison between the two gives MSE = 0.13) with a 1.573 eV band-gap energy.

3.3.4. Sample grown at 350°C

For the C-350 sample seven incidence angles are used and the fitting dielectric function is a free parameter to vary with the same physical assumptions as before. Besides the mixed layer, the optimal overlayer structure includes a roughness layer between the mixed layer and the film, which has a strong influence on the final MSE (Fig. 4(c)). This could physically represent the small film roughness due to

nanocrystallinity, as shown in Fig. 2(c) and Table 1. Despite the low MSE, the fitted thickness of the roughness layer is larger than expected from AFM and the correlation error is high, possibly because of a contribution from the smaller-sized nanospheres to this layer. The Tauc band-gap energy of the film is estimated to 1.1 eV.

3.3.5. Sample grown at 425°C

Modeling the surface overlayer of the C-425 sample did not give meaningful results. This is probably due to the strong depolarization effect of the rough inhomogeneous surface (Fig. 2(d)). To avoid the problem, the ellipsometry measurement was performed from the glass side of the sample (Fig. 4(d)), only fitting the spectral region above 2.2 eV where light is completely absorbed in the film and reflections from the surface overlayer are not contributing to the detected signal. Seven angles of incidence are used and the dielectric function is again fitted freely starting from the C-350 dielectric function.

3.3.6. Dielectric functions

The dielectric functions of the bulk film layer as obtained from the previous analysis are shown in Fig. 6. Those obtained for the two samples deposited at 25°C have very similar shapes and band gap energies. This fact suggests that film thickness does not significantly influence the extracted dielectric functions of the material and the initial assumption of a non-graded layer is confirmed. Also, since the bulk film layer was accurately modeled by a dielectric function featuring a single Tauc-Lorentz oscillator, significant contributions from phases other than CZTS are unlikely. As the deposition temperature is increased, the dielectric functions exhibit more complex dispersion due to increased crystalline order. Unlike in amorphous materials, the selection rule of wave-vector conservation must be applied to optical absorption in crystalline solids, which gives rise to critical point structures at photon energies corresponding to singularities in the joint density of states for a specific wave vector.

Absorption is enhanced in the low- or high-energy neighborhood of a critical point according to its classification [12], therefore critical points can in principle be resolved by analysis of the imaginary part of the dielectric function $\varepsilon_2(E)$. The critical point structures we observe are similar to those reported in two other ellipsometry studies for a single-phase CZTS film [6] and for a CZTS bulk crystal [3], which in turn are in reasonable agreement with theoretical predictions [13]. The C-425 sample exhibits a rather sharp M_1 critical point [12] just below 3 eV, probably corresponding to a critical point of the same type found at 2.92 eV by [6] and at 2.82 eV by [3]. The absorption onset observed in the C-425 sample just above 4 eV may correspond to the M_0 critical point found at 3.92 eV by [6] and at 3.86 eV by [3]. In the 4.5-6.0 eV spectral region, $\varepsilon_2(E)$ in the C-425 sample has four inflection points, possibly arising from a number of broad excitonic critical points as assumed in [6]. The C-350 sample is different from the C-425 sample in the following: 1) broader critical point features, 2) larger values of $\varepsilon_2(E)$ at all photon energies, and 3) red shift (by 0.3-0.5 eV) of the critical point features. The first two differences are probably due to the C-350 film being only partially crystallized, which partially removes the selection rule of wave-vector conservation in optical transitions. The third difference could be due to a global shift of the valence band with respect to the conduction band in the Brillouin zone, thereby shifting the characteristic energy of all optical transitions. It is difficult to estimate how much the presence of SnS and Cu_3SnS_4 in the film bulk affects the dielectric functions of the C-350 and C-425 films. Nevertheless, critical points previously reported for single-phase CZTS have also been identified in our samples. Hence, the effect of secondary phases is not believed to be strong enough to distort the main features of CZTS dielectric functions.

Conclusions

Cu_2ZnSnS_4 films were deposited by PLD in a range of temperatures and thicknesses. From AFM and Raman measurements, it was found that the surface overlayer featured both a complex surface topography and a different phase mix than the underlying film, which can complicate ellipsometry data interpretation. A satisfactory model was proposed for a thin film deposited at room temperature, which was able to accurately reproduce results from topographic measurements and corroborate assumptions from phase analysis. Even though the surface overlayer in the other films is too complex to be able to identify surface phases, dielectric functions were extracted for all films with the exception of the spectral region < 2.2 eV for the film deposited at 425°. The dielectric functions of two films with different thicknesses deposited at room temperature were compatible with an amorphous material with 1.5-1.6 eV band-gap energy and showed no significant thickness dependency. As the deposition temperature was increased, the dielectric functions of the films exhibited additional critical points related to strong optical transitions at specific points of the Brillouin zone. The inclusion of secondary phases in the bulk of the films did not prevent identification of critical points previously reported for CZTS.

Acknowledgements

This work has been supported by a grant from the Danish Council for Strategic Research. CINF is funded by the Danish National Research Foundation (DNRF54).

References

[1] B. Shin, O. Gunawan, Y. Zhu, N.A. Bojarczuk, S.J. Chey, S. Guha, Thin film solar cell with 8.4% power conversion efficiency using an earth-abundant Cu 2 ZnSnS 4 absorber, Prog. Photovoltaics Res. Appl. 21 (2011) 72–76.

[2] W. Wang, M.T. Winkler, O. Gunawan, T. Gokmen, T.K. Todorov, Y. Zhu, D. Mitzi, Device Characteristics of CZTSSe Thin-Film Solar Cells with 12.6% Efficiency, Adv. Energy Mater. 4 (2014) 1301465.

[3] S. Levcenko, G. Gurieva, M. Guc, A. Nateprov, Optical constants of Cu2ZnSnS4 bulk crystals, Mold. J. Phys. Sci. 8 (2009) 173–177.

[4] W. Li, K. Jiang, J. Zhang, X. Chen, Z. Hu, S. Chen, L. Sun, J. Chu, Temperature dependence of phonon modes, dielectric functions, and interband electronic transitions in Cu2ZnSnS4 semiconductor films., Phys. Chem. Chem. Phys. 14 (2012) 9936–41.

[5] L. Sun, J. He, Y. Chen, F. Yue, P. Yang, J. Chu, Comparative study on Cu2ZnSnS4 thin films deposited by sputtering and pulsed laser deposition from a single quaternary sulfide target, J. Cryst. Growth. 361 (2012) 147–151.

[6] J. Li, H. Du, J. Yarbrough, A. Norman, K. Jones, G. Teeter, F. L. J. Terry, D. Levi, Spectral optical properties of Cu2ZnSnS4 thin film between 0.73 and 6.5 eV., Opt. Express. 20 Suppl 2 (2012) A327–332.

[7] J. Alvarez-Garcia, V. Izquierdo-Roca, A. Perez-Rodriguez, Raman spectroscopy on thin films for solar cells, in: D. Abou-Ras, T. Kirchartz, U. Rau (Eds.), Advanced Characterization Techniques for Thin Film Solar Cells, Wiley-VCH Verlag, Wenheim, 2011: pp. 365–386.

[8] H. Fujiwara, Spectroscopic Ellipsometry - Principles and Applications, Wiley, 2007.

[9] J. Tauc, R. Grigorovici, A. Vancu, Optical Properties and Electronic Structure of Amorphous Germanium, Phys. Status Solidi. 15 (1966) 627–637.

[10] S.V. Bagul, S.D. Chavhan, R. Sharma, Growth and characterization of CuxS (x=1.0, 1.76, and 2.0) thin films grown by solution growth technique (SGT), J. Phys. Chem. Solids. 68 (2007) 1623–1629.

[11] F. Zhuge, X. Li, X. Gao, X. Gan, F. Zhou, Synthesis of stable amorphous Cu2S thin film by successive ion layer adsorption and reaction method, Mater. Lett. 63 (2009) 652–654.

[12] C.F. Klingshirn, Semiconductor Optics, Springer-Verlag, Berlin Heidelberg, 1995.

[13] H. Zhao, C. Persson, Optical properties of Cu(In,Ga)Se2 and Cu2ZnSn(S,Se)4, Thin Solid Films. 519 (2011) 7508–7512.

List of tables

[1] Topographic characteristics of CZTS films, measured with a profiler, AFM, and ellipsometry

sample	film thickness [nm]		overall roughness [nm]		film roughness [nm]		overlayer thickness [nm]	MSE
	profiler	ellipsometry	AFM	profiler	AFM	ellipsometry	ellipsometry	
C-25t	190	195	15	15	0.9	0	53	4.0
C-25T	750	733	57	60	1.2	0	74	12.2
C-350	390	379	35	44	2.6	13	180	5.5
C-425	760	770	96	101	96	n.a.	n.a.	2.7

List of figures

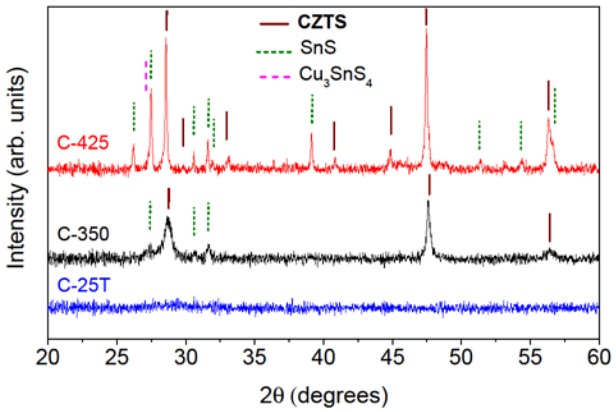

Figure 1

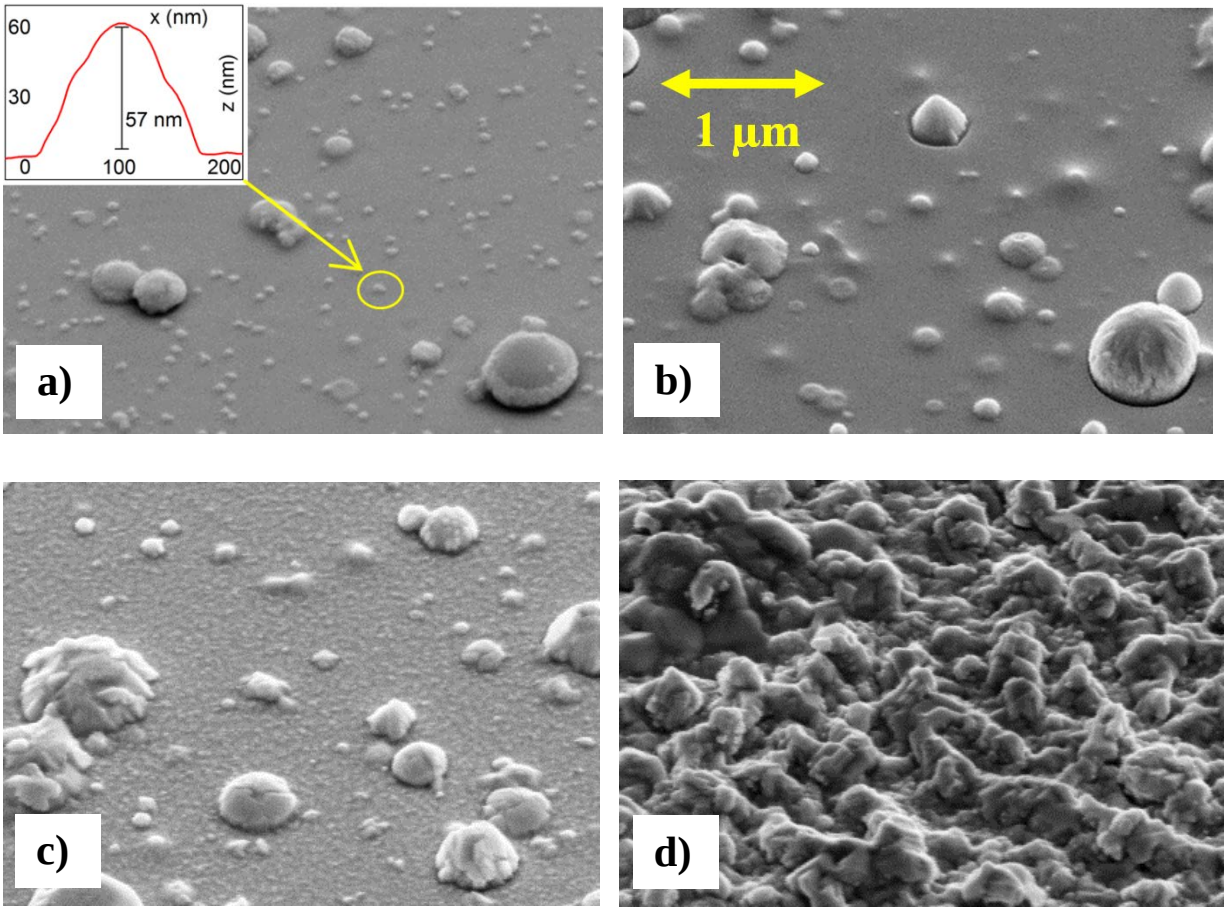

Figure 2

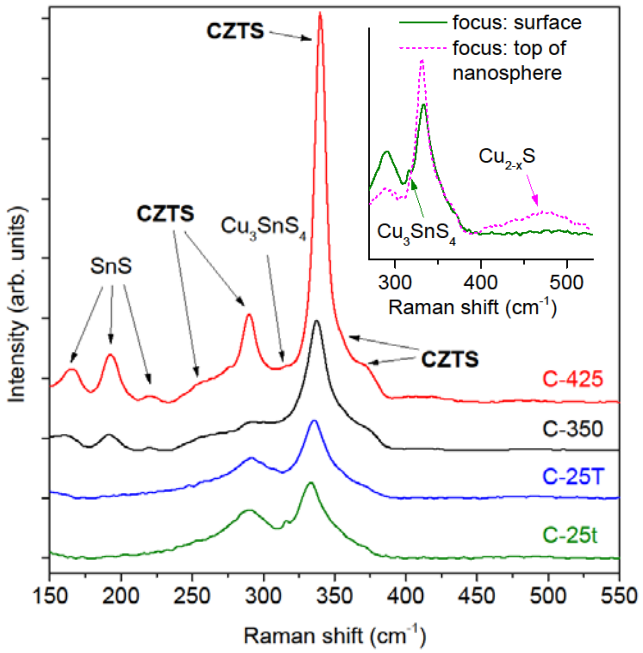

Figure 3

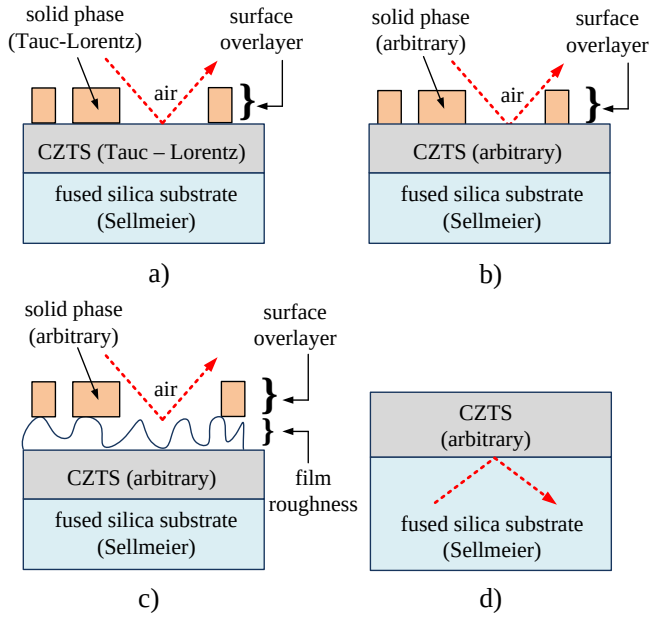

Figure 4

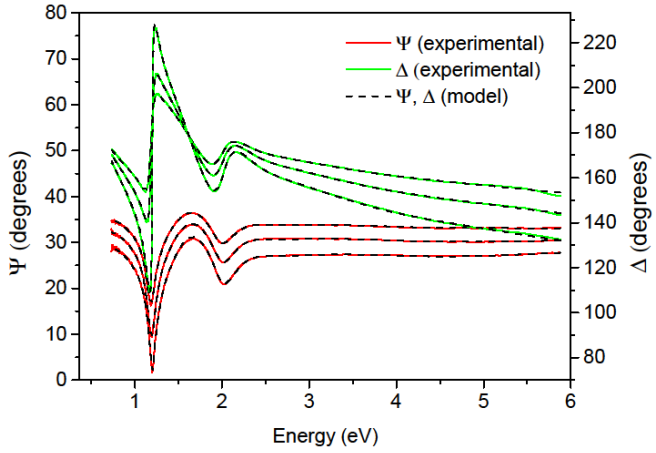

Figure 5

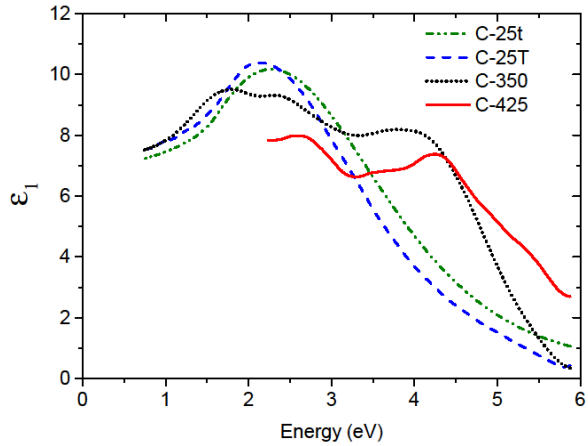

a)

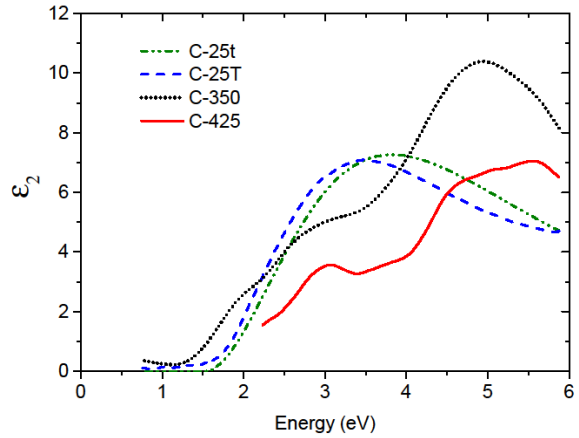

b)

Figure 6

List of figure captions

Figure 1: XRD patterns of the four CZTS films. Only one pattern is shown for the C-25t and C-25T samples, as their differences are negligible. Phase analysis is performed based on peak position and on comparison with Raman spectra. A Cu_3SnS_4 peak is identified as a shoulder in one of the SnS peaks.

Figure 2: SEM images of CZTS films (beam voltage: 5 kV, magnification: 50000X) with a 45° tilt. The scale is the same in all images. **a)** C-25t, where the inset graph shows an AFM scan of one of the smaller nanostructures, about 57 nm in height; **b)** C-25T; **c)** C-350, where a nanocrystalline grain structure becomes visible; **d)** C-425, where surface characteristics are completely changed.

Figure 3: Raman spectra of the four CZTS films. Phase analysis is performed based on peak position. Inset graph: two Raman spectra taken on the C-25t sample. When the laser is focused on top of a nanosphere instead of on the film surface, a Cu_3SnS_4 peak disappears and a $Cu_{2-x}S$ peak appears.

Figure 4: Layer stacks used as optical models for fitting ellipsometry data. **a)** C-25t, **b)** C-25T, **c)** C-350, **d)** C-425. The type of dielectric function used to model each layer is specified in parenthesis. The dashed red lines denote incident and reflected light in the measurement.

Figure 5: Spectral magnitude (Ψ) and phase (Δ) of the ratio between p- and s- type polarization reflection coefficients, measured by ellipsometry at 45, 50 and 55° on the C-25t sample. Solid colored lines: measured spectra. Dashed lines: fitted spectra. The MSE is 4.0.

Figure 6: a) Real part and **b)** imaginary parts of the dielectric functions $\varepsilon = \varepsilon_1 + i\,\varepsilon_2$ extracted by spectroscopic ellipsometry for the four CZTS films. Only the spectral region above 2.2 eV is fitted in the C-425 film due to complications arising when the surface overlayer contributes to the spectrum.